

U.S. Department of Commerce
National Oceanic and Atmospheric Administration
National Weather Service
National Centers for Environmental Prediction
5830 University Research Court
College Park, MD 20740-3818

Office Note 501

<https://doi.org/10.25923/egap-ev04>

SOLVING THE LAPLACE EQUATION IN A RIGHT-ANGLED BICORN AND
CONSTRUCTING SMOOTH BLENDING FUNCTIONS FOR CONFORMAL
OVERSET GRIDS

R. James Purser*
IM Systems Group, Rockville, Maryland

March 18, 2020

THIS IS AN UNREVIEWED MANUSCRIPT, PRIMARILY INTENDED FOR INFORMAL
EXCHANGE OF INFORMATION AMONG THE NCEP STAFF MEMBERS

* email: jim.purser@noaa.gov

Abstract

A significant problem very often encountered when using a polyhedral grid framework for global numerical weather simulation is the ‘imprinting’ of spurious computational noise that occurs in the pattern of the edges and vertices of the chosen polyhedral geometry. Smoothing the grid across edges only partially mitigates the problem since the singularities still persist at the vertices. A more complete solution of this difficulty can be obtained by employing a composite overset grid configuration where two or more large grid domains overlap to cover the globe without singularities or regions of strong grid curvature. The redundancy of solutions in the overlap regions is then resolved by interpolations and progressive blending. It is preferable, for numerical reasons, to choose a grid that is orthogonal, especially if it possesses the additional desirable attribute of being conformal, provided this can be done in such a way that the resolution remains approximately uniform. A special class of these overset grids employs the idea of a two-sheeted Riemann surface, which enables the overlap regions of a conformal grid to be restricted to small two-cusp ‘bicorn’ areas very close to the polyhedron’s original vertices. At the cusps of each bicorn are a pair of ‘branch points’ of the mapping between the space of the grid and the geographical domain. While being the only singular points in the used part of the computational grid, these branch points still preserve continuity of several derivatives of the mapping and therefore behave as if they are effectively nonexistent as far as the model numerics are concerned. This note describes a general method of constructing the blending function for reconciling the two solutions in each bicorn based upon the principle of solving a Laplace equation for a ‘potential’ there (which is a valid solution to the Laplace equation in both sheets’ conformal coordinates) and deriving the weights as incomplete beta functions of that potential, in order to achieve a high degree of smoothness on the bounding edges of the bicorn.

1. Introduction

All of the traditional polyhedral grids, but especially the increasingly popular cubic families of grids used for numerical weather simulation, are known to exhibit spurious ‘grid imprinting’ effects in their extended forecasts or climatology. This occurs mainly because these grids possess discontinuities in their properties along the edges of the cube, and more particularly at the vertices. The gnomonic cubic grid was introduced for numerical modeling by Sadourny (1972) and minor modifications of it were considered by Ronchi et al. (1996), Rančić et al. (1996), Putman and Lin (2007), and others. The article by Rančić et al. (1996) also introduced the conformal cubic grid, which removed the edge discontinuity, but left a singularity at each vertex. In the vicinity of each vertex, the resolution became excessively high, which is clearly problematic for a model with explicit dynamics (though not so much for a semi-implicit semi-Lagrangian model such as the one introduced by McGregor (1996) to exploit this grid). A more generalized parameterized family of ‘smooth cubic’ grids (containing the conformal one as a special extreme case) was introduced by Purser and Rančić (1998) and enabled a much more uniform resolution of grid to be obtained. This family culminated in the extreme case of the

‘Uniform Jacobian’ grid tested in the context of the NMMB model (Janjić and Gall 2012) by Rančić et al. (2017). Unfortunately, the more uniform resolution led to an exacerbation of the excessive curvature that these grids suffer from in the vicinity of the eight vertices, and the application of customized numerics there to address this anticipated problem was insufficient to entirely remove the persisting grid imprinting visible at these places.

An alternative tactic, which has a much higher chance of eliminating the grid imprinting, although at the cost of a greater numerical complexity and the need for accurate interpolations along a broad swath of the the globe, is to use two or three overlapping or ‘overset’ grids, each of a limited area kind without coordinate singularities anywhere within or near their region of application, and to reconcile their solutions every time step by mutual interpolation and appropriately weighted blending of the redundant portions of the solution. Probably the first approach of this kind was the method proposed by Phillips (1957) using two polar stereographic grids overlapping a central cylindrical map grid. The method of overset grids was developed especially by Starius (1980), Chesshire and Henshaw (1990) and Browning et al. (1989). As proposed by Kageyama and Sato (2004), the globe can be covered, with relatively little distortion, using a congruent pair of elongated rectangular domains oriented transversally to one another in the so-called ‘Yin-Yang’ configuration. The overlapping region is then a single sinuous zone resembling the seam of a baseball ball.

In the context of regions each gridded with a square mesh, we recognize that, along substantial stretches of the overlap regions of these various overset grids, the two overlapping meshes can be made to coincide without much further distortion. This is true of both the Yin-Yang grid and of the three-grid configuration proposed by Phillips, suggesting that, apart from eight isolated corner regions, the grids can actually be made perfectly continuous. Furthermore, by the careful construction of conformal mappings that involve two-sheeted Riemann surfaces winding around branch-point weak singularities, it becomes possible to combine the best features of the conformal grids with those of the overset grids in such a way that the amount of mutual interpolation and blending involved is minimal. A Riemann surface is a complex manifold, associated with some complex analytic function which would allow more than one solution on the ordinary complex plane, but which becomes single-valued on this manifold. It can have a non-trivial topology, and is a concept found throughout the field of complex function theory (Weyl, 2009; Napier and Ramachandran, 2011; Krantz, 2016) and even in discrete group theory, for example, in Beardon (1983, Chap. 6). Our application locally requires only consideration of simple two-sheeted varieties of Riemann surfaces, as will be made clear in the following sections. Corresponding to the Phillips-type overset configuration we have a conformal ‘barrel’ or ‘drum’ conformal grid exemplified by the construction shown in Fig. 1.

We leave the description of the construction of this and similar conformal overset grids to another note (Purser and Rančić , 2020). What will concern us here is the question of how best to define the blending weights by which the two solutions should be combined in the eight compact ‘bicorn’ regions near what would be the singular corners of the standard conformal cube. Owing to the transitivity of conformal mappings, it seems very natural to seek a solution to this question involving a conformal mapping of this region to a parallel-sided strip, since this will imply the strip is conformally mapped to *both* of the map domains simultaneously. The contours of the mapping which, in the strip-domain, would be the lines parallel to the sides of the strip, can then be taken to be the contours of the blending weights themselves. In fact,

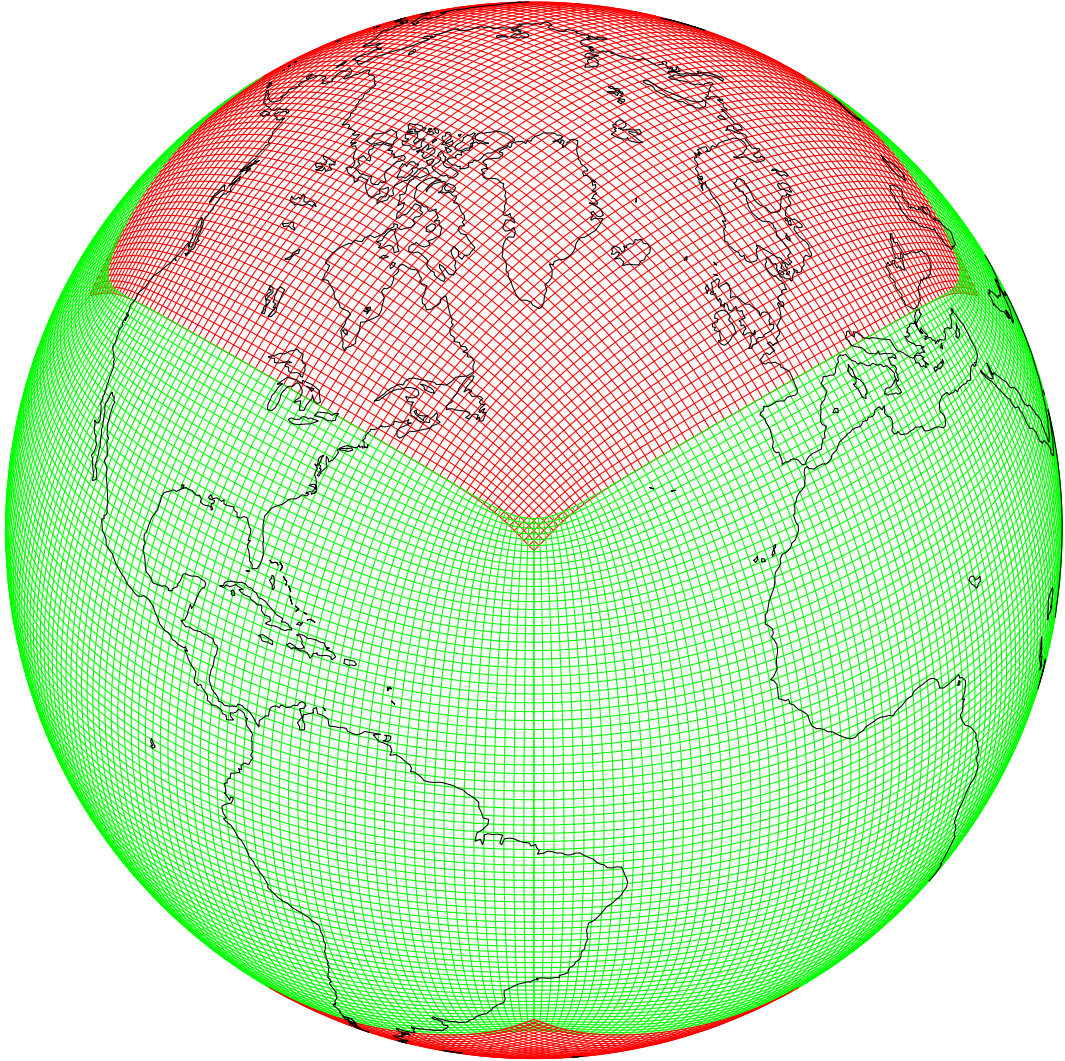


Figure 1. An example of a conformal overset grid based on cubic geometry. The symmetry is broken by the overlapping regions, the reduced symmetry being that of a solid square dihedron, or square prism (with a symmetry group of order 16). It is also possible to construct a superficially similar conformal overset Yin-Yang cubic grid, with the smaller resulting symmetry (of order 8).

if we take the strip to run with its transverse coordinate y between 0 and 1, a good choice of blending weights would be those that are the incomplete beta function, of a chosen symmetrical degree, m , defined (see Abramowitz and Stegun, 1972, article 26.5.1, p944):

$$W(y) \equiv I_y(m, m) = \frac{1}{B(m, m)} \int_0^y t^{m-1} (1-t)^{m-1} dt, \quad (1.1)$$

where $B(a, b)$ is the two-parameter Euler beta function. This weight would apply to the solution of one of the overlapping regions; the complement, $1 - W(y)$, would supply the weight for the other solution at the same geographical location. Examples of such beta function weights for

parameters $m = 2$ and $m = 3$ are:

$$W(y) = 3y^2 - 2y^3, \tag{1.2}$$

which ensures continuity up to the first derivative, or

$$W(y) = 10y^3 - 15y^4 + 6y^5, \tag{1.3}$$

which ensures continuity up to the second derivative of weight W , except at or beyond the cusps of the bicorn, of course. The ‘branch points’ at the two cusps of the bicorn are weak singularities of the mapping in the sense that only high order derivatives of it become discontinuous. Therefore, it is not necessary for the blending weights to be smoothly continuous on a transect through these special points since the two solution fields they modulate become identical at these limiting points.

In physical terms, we can think of the solution for the implied spatial function y that we seek as being equivalent to the electrostatic potential resulting from one side ($y = 0$) of the bicorn being a ‘conductor’ at zero ‘potential’, while the other side ($y = 1$), also a conductor, is maintained at a unit potential, in a problem of two-dimensional electrostatics. The rest of this note will focus on approximate solutions to just this special class of problems that are valid when the curved boundary of the bicorn is smooth and the bicorn itself is a relatively slender region, as it is in the overlap shown in Fig. 1.

2. Outline

The region we call a ‘bicorn’ is assumed to lie in the positive quadrant of a cartesian plane, with cusps at $(1, 0)$ and $(0, 1)$, straight edge boundaries between these points and the origin, and a smooth curved boundary $(p, q) = \mathbf{G}(s)$ in the interior of the positive quadrant that links the cusp points. Thus, if we take complex $Z = (p + iq)^2 \equiv (X + iY)$, this somewhat awkward region becomes transformed into a ‘hill’ or ‘bell’ in the positive- Y half-plane between transformed cusps on the X -axis at $X = \pm 1$, and the former bounding curve \mathbf{G} becomes transformed into a new bell-shaped curved boundary, $Z = S(s)$. This can be thought of as a very trivial special case of the Schwarz-Christoffel mapping, which has numerous practical applications (Driscoll and Trefethen 2002). Owing to the transitivity of conformal mappings, a solution in the Z -plane implies one in the original bicorn domain, but the Z -plane region (without a corner) is much easier to work in. Although there is no restriction in principle to the validity of the method we describe, we shall assume the symmetry of the problem about the imaginary Z axis (or about the line $p = q$ in the original problem).

The idea now is to seek a conformal mapping between the doubly-infinite unit strip in another complex plane, of variable $z = (x + iy)$, where $x \in (-\infty, \infty)$ and $y \in [0, 1]$, to the bell-shaped image of the bicorn in the complex plane of Z . If the solution domain has the aforementioned mirror symmetry, we can express this solution as a complex Fourier transform:

$$Z(z) = Bz + \int_0^\infty F(k) \sin(kz) dk, \tag{2.1}$$

with real scaling factor, B , and real coefficients $F(k)$. Then we can approximate the solution for a finite portion by using a fast Fourier transform (FFT), if the sufficiently resolved coefficients $F(k)$ are given at uniform intervals of positive wavenumber k . Note that

$$\sin(kz) = \sin(kx) \cosh(ky) + i \cos(kx) \sinh(ky), \quad (2.2)$$

so the coefficients $F_j = F(j\delta k)$ can be found by ordinary FFT analysis of the solution $X_0(x)$ if this solution is given along the real axis $y = 0$ at a set of uniformly spaced x (assuming we can adequately deal with the technicality of requiring the numerical approximating solution to be periodic, which we can generally do without incurring large error simply by making the period in x finite but very large compared to the unit-width of the strip).

We make a further assumption that the boundary curve S is very smooth on the scale of its height above the real axis, since this will allow us to make a preliminary asymptotic approximation to the solution for $X_0(x)$ based on the height and first few derivatives of S at this same X -coordinate. Once we have a sufficiently good approximation to the real function $X_0(x)$, and hence the corresponding Fourier coefficients for the whole interior solution, we can examine the mismatch between the $y = 1$ edge of the approximate solution, $Z_1(x + i) = (X_1(x + i) + iY_1(x + i))$, and the known boundary location S . This is quantified in terms of \mathcal{L} , the integrated squared-distance between the two curves when the integral is with respect to parameter s . Then we minimize this quantity with respect to variations in both the scaling factor, B , and in the discrete Fourier sine coefficients F_j , to find the desired solution whose edge conforms to the curve S . But in most practical cases, it looks as if the asymptotic approximation can be made accurate enough just by itself, which is why much of this note is devoted to the examination of the asymptotic method.

In the next section, we describe how the derivatives of the boundary curve, $S(s) = X(s) + iY(s)$, with respect to the smooth parameter s can be converted into corresponding expressions for the derivatives of Y with respect to X . In section 4 we introduce the method by which the asymptotic expansion coefficients are obtained for an increasing index parameter λ that labels each successive set of terms in a systematic progression of higher ‘orders’. Finally, we discuss the prospects for extending these techniques to the cases of more traditional overset topologies, except with the restriction that the grids in each map panel are of the conformal kind.

3. Convenient notations for the manipulation of derivatives of a parameterized curve

If X and Y are quantities (such as the real and imaginary parts of a complex quantity) of similarly dimensioned units and given as smooth functions of the common dimensionless parameter s , and if we want to relate the higher derivatives of Y with respect X in nondimensional terms, then it will be convenient to use Y in the nondimensionalizing normalizations. A convenient notation for these nondimensional derivatives is:

$$D_k \equiv Y^{k-1} \frac{d^k Y}{dX^k}. \quad (3.1)$$

TABLE 1. COEFFICIENTS OF THE FAÀ DI BRUNO COEFFICIENTS, B , AND THOSE FOR THE INVERSE FORMULAS, C , FOR THE FIRST FEW PARTITION

π	$B\pi$	$C\pi_{,1}$	$C\pi_{,2}$	$C\pi_{,3}$	$C\pi_{,4}$	$C\pi_{,5}$	$C\pi_{,6}$
0		1	1	1	1	1	1
1	1		-1	-3	-6	-10	-15
2	1			-1	-4	-10	-20
1, 1	1			3	15	45	105
3	1				-1	-5	-15
2, 1	3				10	60	210
1, 1, 1	1				-15	-105	-420
4	1					-1	-6
3, 1	4					15	105
2, 2	3					10	70
2, 1, 1	6					-105	-840
1, 1, 1, 1	1					105	945
5	1						-1
4, 1	5						21
3, 2	10						35
3, 1, 1	10						-210
2, 2, 1	15						-280
2, 1, 1, 1	10						1260
1, 1, 1, 1, 1	1						-945

We also define the nondimensional derivatives,

$$p_k = \frac{1}{Y} \frac{d^k X}{ds^k} \quad (3.2a)$$

$$q_k = \frac{1}{Y} \frac{d^k Y}{ds^k}. \quad (3.2b)$$

Another notational convenience is obtained by abbreviating products of such terms in the same family by employing index vectors according to the rule,

$$D_{q_1 \dots q_m} \equiv \prod_{i=1}^m D_{j_i}, \quad (3.3)$$

and similarly for p and q quantities.

By the chain rule:

$$q_1 = D_1 p_1, \quad (3.4a)$$

and, extending to some of the higher order terms:

$$q_2 = D_1 p_2 + D_2 p_{1,1}, \quad (3.4b)$$

$$q_3 = D_1 p_3 + 3D_2 p_{2,1} + D_3 p_{1,1,1}, \quad (3.4c)$$

leads to the general formula of Faà di Bruno type:

$$q_n = \sum_{k=1}^n D_k \left[\sum_{\boldsymbol{\pi} \in \Pi_n^k} B_n p_{\boldsymbol{\pi}} \right], \quad (3.5)$$

where each index *vector* $\boldsymbol{\pi}$ corresponds to a ‘partition’ and Π_n^k denotes the set of partitions of n into exactly k parts. We adopt the arbitrary convention that the indices in each partition are nonincreasing, as in the middle term of (3.4c). The Faà di Bruno coefficients $B_{\boldsymbol{\pi}}$ are listed for the first few nonempty partitions in table 1 and their combinatorial definition as multinomial coefficients can be found in Abramowitz and Stegun (1972).

These formulas can be inverted systematically to obtain the D_n from all the p_k and q_k with $k \leq n$ but, in order to express to resulting inverse formulas, it is convenient first to define the modified nondimensional quantities,

$$\hat{q}_k = \frac{q_k}{p_1^k} = Y^{k-1} \frac{d^k Y}{ds^k} \left(\frac{dX}{ds} \right)^{-k}, \quad (3.6)$$

and

$$\tilde{p}_k = \frac{p_{k+1}}{p_1^{k+1}} = Y^k \frac{d^{k+1} X}{ds^{k+1}} \left(\frac{dX}{ds} \right)^{-(k+1)}. \quad (3.7)$$

We also allow the index vector of the \tilde{p} to include the null index, i.e., $\tilde{p} \equiv \tilde{p}_0 = 1$, that corresponds to the single null partition. With these definitions, the first few of the inverse formulas can be written explicitly:

$$D_1 = \hat{q}_1 \tilde{p} \quad (3.8a)$$

$$D_2 = \hat{q}_2 \tilde{p} - \hat{q}_1 \tilde{p}_1 \quad (3.8b)$$

$$D_3 = \hat{q}_3 \tilde{p} - 3\hat{q}_2 \tilde{p}_1 + \hat{q}_1 (-\tilde{p}_2 + 3\tilde{p}_{1,1}), \quad (3.8c)$$

and the general formula given by:

$$D_n = \sum_{k=0}^{n-1} \hat{q}_{n-k} \left[\sum_{\boldsymbol{\pi} \in \Pi_k} C_{\boldsymbol{\pi}, n} \tilde{p}_{\boldsymbol{\pi}} \right], \quad (3.9)$$

where the set of *all* partitions of n is Π_n (including the null partition when $n = 0$), and the coefficients $C_{\boldsymbol{\pi}, n}$ are listed, for the first few n , in the same table 1.

When we compound the D_k to form various partition-associated products it becomes natural to group into vectors those combinations that associate with partitions of the same n . Thus, we define vectors:

$$\mathbf{D}_{(1)} = [D_1]^T \quad (3.10a)$$

$$\mathbf{D}_{(2)} = [D_2, D_{1,1}]^T \quad (3.10b)$$

$$\mathbf{D}_{(3)} = [D_3, D_{2,1}, D_{1,1,1}]^T \quad (3.10c)$$

$$\mathbf{D}_{(4)} = [D_4, D_{3,1}, D_{2,1}, D_{2,1,1}, D_{1,1,1,1}]^T \quad (3.10d)$$

$$\mathbf{D}_{(5)} = [D_5, D_{4,1}, D_{3,2}, D_{3,1,1}, D_{2,2,1}, D_{2,1,1,1}, D_{1,1,1,1,1}]^T. \quad (3.10e)$$

In the practical application of this formalism that we develop in the next section to obtain asymptotic series, we shall use the fact that the same nondimensional derivatives D_k can be obtained from two or more parameters corresponding to the ‘ s ’ we have used here. We shall particularly consider the case where the $X(s)$ and $Y(s)$ correspond to the smooth boundary curve of the solution domain of the region in which we wish to solve the two-dimensional Laplace equation with this boundary defining one of the potentials. But since the complex combination, $Z(z) = X(z) + iY(z)$ as a function of the complex z defines a conformal mapping between the (X, Y) solution domain and the infinite unit-width strip of $z = x + iy$, then we can also think of the boundary values $X_1(x) = X(x + i)$ and $Y_1(x) = Y(x + i)$ as being given as functions of the alternative parameter, x .

4. Asymptotic series to estimate dX_0/dx

If we can estimate the x -derivative of X_0 , we can easily integrate it numerically to obtain $X_0(x)$ itself, which is all we need to imply the whole solution. With a shift of origin, we can assume it is the derivative at $x = 0$ that we are trying to estimate, and we can therefore expand the solution locally as a Taylor series (remembering that we can no longer invoke the mirror symmetry assumption, though, with this shifted origin). In preparation for an asymptotic analysis, we can assume that the coefficient of the m th derivative is of a smaller order than unity by a factor λ^{m-1} . With this symbolic rescaling, the real Taylor series coefficients can be taken to have order of magnitude $a_i \sim 1$ in the expansion in which the smallness of the successive terms is indicated explicitly by the appropriate power of λ :

$$X_0 = a_1x + \lambda a_2x^2/2 + \lambda^2 a_3x^3/6 + \mathcal{O}(\lambda^3). \quad (4.1)$$

It is algebraically convenient in the following derivations to define ratios:

$$c_k = \frac{a_{k+1}}{a_1} \quad k \geq 0, \quad (4.2)$$

so that (4.1) is equivalently written:

$$X_0 = a_1 \left[x + \lambda c_1 x^2/2 + \lambda^2 c_2 x^3/6 \right] + \mathcal{O}(\lambda^3) \quad (4.3a)$$

$$\equiv a_1 \sum_{k=1}^{\infty} \lambda^{k-1} c_{k-1} \frac{x^k}{k!}. \quad (4.3b)$$

For the solution Z_1 at the upper edge, where $y = 1$, we must use the fully complex-valued powers of $(x+i)$ to obtain the real (X_1) and imaginary (Y_1) parts of the complex answer. We can express the k th derivative with respect to x in formulas of similar forms in the following unified way, using binomial expansions of the components, x and i in the powers, $(x + i)^k$:

$$\frac{d^k X_1}{dx^k} = a_1 \left[\lambda^{k-1} c_{k-1} R_0 + \lambda^k c_k R_1 + \dots \right] \quad (4.4a)$$

$$\frac{d^k Y_1}{dx^k} = a_1 \left[\lambda^k c_k Q_1 + \lambda^{k+1} c_{k+1} Q_2 + \dots \right], \quad (4.4b)$$

where R_k has for its first few examples,

$$R_0 = 1 \quad (4.5a)$$

$$R_1 = x \quad (4.5b)$$

$$R_2 = -\frac{1}{2} + \frac{x^2}{2} \quad (4.5c)$$

$$R_3 = -\frac{x}{2} + \frac{x^3}{6} \quad (4.5d)$$

$$R_4 = \frac{1}{24} - \frac{x^2}{4} + \frac{x^4}{24}, \quad (4.5e)$$

or generally:

$$R_k = \frac{1}{k!} \sum_{\ell=0}^{\lfloor k/2 \rfloor} (-1)^\ell \binom{k}{2\ell} x^{k-2\ell} \quad (4.6)$$

and Q_k has for its first few examples,

$$Q_0 = 0 \quad (4.7a)$$

$$Q_1 = 1 \quad (4.7b)$$

$$Q_2 = x \quad (4.7c)$$

$$Q_3 = -\frac{1}{6} + \frac{x^2}{6} \quad (4.7d)$$

$$Q_4 = -\frac{x}{6} + \frac{x^3}{6}, \quad (4.7e)$$

or generally,

$$Q_k = \frac{1}{k!} \sum_{\ell=0}^{\lfloor k/2 \rfloor} (-1)^\ell \binom{k}{2\ell+1} x^{k-2\ell-1}. \quad (4.8)$$

If we look only at the first three terms of the expansion for X_1 itself (i.e., $k=0$ in (4.4a)), then

$$X_1 = a_1 \left[x + \lambda c_1 \left(-\frac{1}{2} + \frac{x^2}{2} \right) \right] + \mathcal{O}(\lambda^2). \quad (4.9)$$

Then the offset $x = \hat{x}$ needed to make X_1 vanish can be made an expansion in powers of λ :

$$\hat{x} = \lambda x_1 + \lambda^2 x_2 + \dots, \quad (4.10)$$

where we immediately see from (4.9) that, in order that the terms in λ vanish,

$$x_1 = \frac{c_1}{2}. \quad (4.11)$$

More generally, if we use the partition-associated notation for vector indices that we introduced in section 3, then including the next higher order term in the expansion for \hat{x} gives:

$$\hat{x} = \lambda \frac{c_1}{2} + \lambda^3 \left(-\frac{c_3}{24} + \frac{c_{2,1}}{4} - \frac{c_{1,1,1}}{8} \right) + \mathcal{O}(\lambda^5), \quad (4.12)$$

where, as a consequence of symmetry, only odd orders of λ appear in the general formal expansion for \hat{x} .

The combinations of the products of c_k that appear in a term at order λ^m are those for which the sum of the k indices equals m . In other words, the vector of combinations of products of c_k at each order λ^m can be deduced from the set of partitions of m , and it is convenient to define such vectors $\mathbf{c}_{(m)}$. The first few of these are given as follows (including the null-partition case, $\mathbf{c}_{(0)}$):

$$\mathbf{c}_{(0)} = 1 \tag{4.13a}$$

$$\mathbf{c}_{(1)} = \lambda[c_1]^T \tag{4.13b}$$

$$\mathbf{c}_{(2)} = \lambda^2[c_2, c_{1,1}]^T \tag{4.13c}$$

$$\mathbf{c}_{(3)} = \lambda^3[c_3, c_{2,1}, c_{1,1,1}]^T \tag{4.13d}$$

$$\mathbf{c}_{(4)} = \lambda^4[c_4, c_{3,1}, c_{2,2}, c_{2,1,1}, c_{1,1,1,1}]^T \tag{4.13e}$$

$$\mathbf{c}_{(5)} = \lambda^5[c_5, c_{4,1}, c_{3,2}, c_{3,1,1}, c_{2,2,1}, c_{2,1,1,1}, c_{1,1,1,1,1}]^T. \tag{4.13f}$$

We can use the notation to write,

$$\begin{aligned} \hat{x} &= \left(\frac{1}{2}\right) \cdot \mathbf{c}_{(1)} + (-1/24, +1/4, -1/8) \cdot \mathbf{c}_{(3)} + \dots \\ &= \sum_{k=1}^{\infty} \mathbf{G}_{2k-1}^T \cdot \mathbf{c}_{(2k-1)}, \end{aligned} \tag{4.14a}$$

for appropriate coefficients vectors, \mathbf{G}_{2k-1} .

Corresponding to this offset \hat{x} that makes $X_1(\hat{x}) = 0$ the value \hat{Y}_1 of Y_1 at that point is found to be:

$$\hat{Y}_1 = a_1 \left[1 + \left(-\frac{1}{6}, \frac{1}{2}\right) \cdot \mathbf{c}_{(2)} + \left(\frac{1}{120}, -\frac{1}{8}, 0, \frac{3}{8}, -\frac{1}{8}\right) \cdot \mathbf{c}_{(4)} \right] + \mathcal{O}(\lambda^6). \tag{4.15}$$

By equating powers of λ we can formally invert this expansion to obtain one for a_1 in terms of \hat{Y}_1 and the components of the vectors $\mathbf{c}_{(k)}$ for even k . The first few terms of this inverted expansion can be written:

$$a_1 = \hat{Y}_1 \left[1 + \mathbf{F}_{(2)}^T \cdot \mathbf{c}_{(2)} + \mathbf{F}_{(4)}^T \cdot \mathbf{c}_{(4)} \right] + \mathcal{O}(\lambda^6), \tag{4.16}$$

where

$$\mathbf{F}_{(2)} = \left(\frac{1}{6}, -\frac{1}{2}\right)^T \tag{4.17a}$$

$$\mathbf{F}_{(4)} = \left(-\frac{1}{120}, \frac{1}{8}, \frac{1}{36}, -\frac{13}{24}, \frac{3}{8}\right)^T \tag{4.17b}$$

Although we already know \hat{Y}_1 (from the specification of the boundary curve) we still have some work to do to get expressions for the components of the vectors $\mathbf{c}_{(k)}$ in terms of quantities that we can diagnose from the definition of the same boundary curve. We proceed by evaluating the

x -derivatives, at \hat{x} , of X_1 and Y_1 using (4.4a) and (4.4b) and applying the methods of section 3 to combine these derivatives into the nondimensionalized vectors $\mathbf{D}_{(k)}$ of products of the derivatives of \hat{Y}_1 with respect to \hat{X}_1 , which the boundary curve determines. We exemplify the process explicitly only for the first few terms in the expansion in powers of λ , but higher order terms can be obtained by a straightforward extension of the same methods, but with greater labor, of course.

When we use the first few terms of \hat{x} to obtain the corresponding approximation for R_k and Q_k and plug these results into the expansion for $d^k X_1/dx^k$ and $d^k Y_1/dx^k$ we find:

$$\frac{1}{a_1} \frac{d\hat{X}_1}{dx} = \left[1 + \left(\frac{1}{2}, -\frac{1}{2}\right) \cdot \mathbf{c}_{(2)} \right] + \mathcal{O}(\lambda^4) \quad (4.18a)$$

$$\frac{1}{a_1} \frac{d^2\hat{X}_1}{dx^2} = \left[1 \cdot \mathbf{c}_{(1)} + \left(-\frac{1}{2}, \frac{1}{2}, 0\right) \cdot \mathbf{c}_{(3)} \right] + \mathcal{O}(\lambda^5) \quad (4.18b)$$

$$\frac{1}{a_1} \frac{d^3\hat{X}_1}{dx^3} = (1, 0) \cdot \mathbf{c}_{(2)} + \mathcal{O}(\lambda^4) \quad (4.18c)$$

$$\frac{1}{a_1} \frac{d^4\hat{X}_1}{dx^4} = (1, 0, 0) \cdot \mathbf{c}_{(3)} + \mathcal{O}(\lambda^5), \quad (4.18d)$$

where the higher order terms can be obtained, if needed, by a mechanical algebraic process.

Similarly for the derivatives of \hat{Y}_1 :

$$\frac{1}{a_1} \frac{d\hat{Y}_1}{dx} = \left[(1) \cdot \mathbf{c}_{(1)} + \left(-\frac{1}{6}, \frac{1}{2}, 0\right) \cdot \mathbf{c}_{(3)} \right] + \mathcal{O}(\lambda^5) \quad (4.19a)$$

$$\frac{1}{a_1} \frac{d^2\hat{Y}_1}{dx^2} = \left[(1, 0) \cdot \mathbf{c}_{(2)} + \left(-\frac{1}{6}, \frac{1}{2}, 0, 0\right) \cdot \mathbf{c}_{(4)} \right] + \mathcal{O}(\lambda^6) \quad (4.19b)$$

$$\frac{1}{a_1} \frac{d^3\hat{Y}_1}{dx^3} = (1, 0, 0) \cdot \mathbf{c}_{(3)} + \mathcal{O}(\lambda^5) \quad (4.19c)$$

$$\frac{1}{a_1} \frac{d^4\hat{Y}_1}{dx^4} = (1, 0, 0, 0, 0) \cdot \mathbf{c}_{(5)} + \mathcal{O}(\lambda^6). \quad (4.19d)$$

In order to apply the methods of section 3 to get derivatives of Y_1 with respect to X_1 , we need the powers of the inverse of dX_1/dx at \hat{x} . The leading terms are just:

$$a_1^k \left(\frac{d\hat{X}_1}{dx} \right)^k = 1 + \left[-\frac{k}{2}, \frac{k}{2} \right] \cdot \mathbf{c}_{(2)} + \mathcal{O}(\lambda^4). \quad (4.20)$$

We now have the ingredients to construct the expansions, correct to order λ^4 , of $\mathbf{D}_{(2)}$ and $\mathbf{D}_{(4)}$, which we can express in matrix form:

$$\begin{bmatrix} \mathbf{D}_{(2)} \\ \mathbf{D}_{(4)} \end{bmatrix} = \begin{bmatrix} \mathbf{M}_{(2,2)} & \mathbf{M}_{(2,4)} \\ \mathbf{0} & \mathbf{M}_{(4,4)} \end{bmatrix} \begin{bmatrix} \mathbf{c}_{(2)} \\ \mathbf{c}_{(4)} \end{bmatrix} + \mathcal{O}(\lambda^6), \quad (4.21)$$

where,

$$\mathbf{M}_{(2,2)} = \begin{bmatrix} 1 & -1 \\ 0 & 1 \end{bmatrix} \quad (4.22a)$$

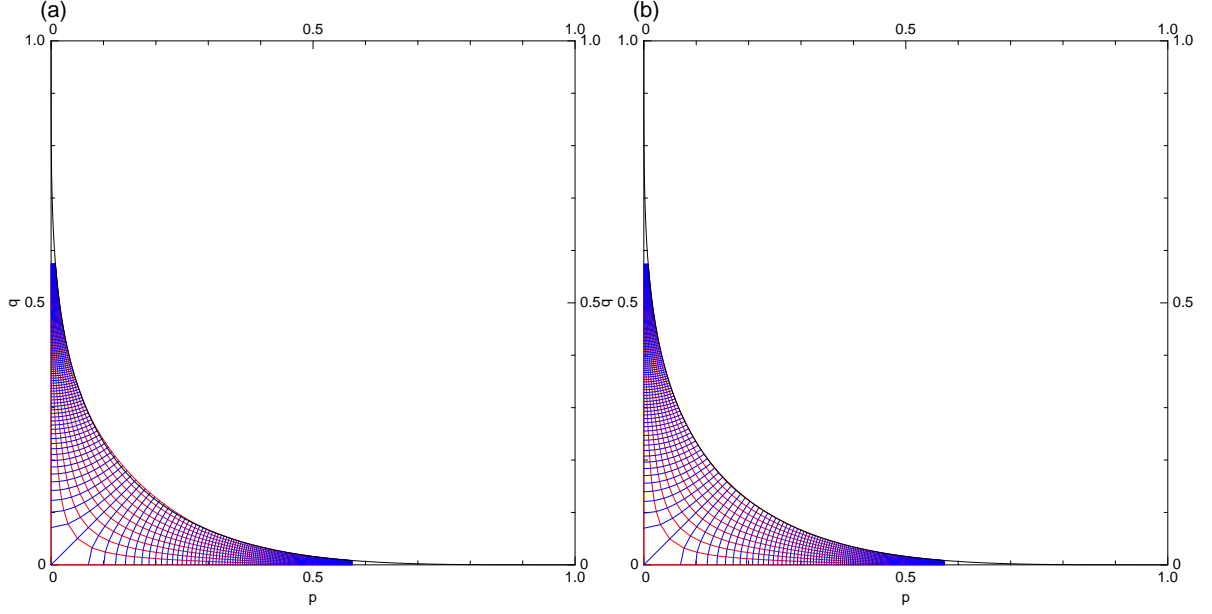


Figure 2. The approximate bicorn solutions obtained using the zeroth-order approximation $a_1 = \hat{Y}_1$ in panel (a), compared to the corresponding improved solution of panel (b) that uses the approximation (4.23) good to order λ^2 .

$$\mathbf{M}_{(2,4)} = \begin{bmatrix} -\frac{1}{6} & \frac{7}{6} & \frac{5}{6} & -\frac{17}{6} & 1 \\ 0 & -\frac{1}{3} & 0 & 2 & -1 \end{bmatrix} \quad (4.22b)$$

$$\mathbf{M}_{(4,4)} = \begin{bmatrix} 1 & -7 & -4 & 25 & -15 \\ 0 & 1 & 0 & -4 & 3 \\ 0 & 0 & 1 & -2 & 1 \\ 0 & 0 & 0 & 1 & -1 \\ 0 & 0 & 0 & 0 & 1 \end{bmatrix}. \quad (4.22c)$$

This upper-triangular, or at least block-upper-triangular, matrix structure persists to higher orders, allowing the inversion of it to each even degree in the formal parameter, λ . Thus, to just second-order, we can now express the asymptotic expansion for a_1 :

$$a_1 = \hat{Y}_1 \left[1 + \mathbf{H}_{(2)}^T \cdot \mathbf{D}_{(2)} \right] + \mathcal{O}(\lambda^4), \quad (4.23)$$

and at fourth order:

$$a_1 = \hat{Y}_1 \left[1 + \mathbf{H}_{(2)}^T \cdot \mathbf{D}_{(2)} + \mathbf{H}_{(4)}^T \cdot \mathbf{D}_{(4)} \right] + \mathcal{O}(\lambda^6), \quad (4.24)$$

where the vectors of coefficients are defined recursively:

$$\mathbf{H}_{(2)}^T = \mathbf{F}_{(2)}^T \mathbf{M}_{(2,2)}^{-1} \quad (4.25a)$$

$$\mathbf{H}_{(4)}^T = \left(-\mathbf{H}_{(2)}^T \mathbf{M}_{(2,4)} + \mathbf{F}_{(4)}^T \right) \mathbf{M}_{(4,4)}^{-1}, \quad (4.25b)$$

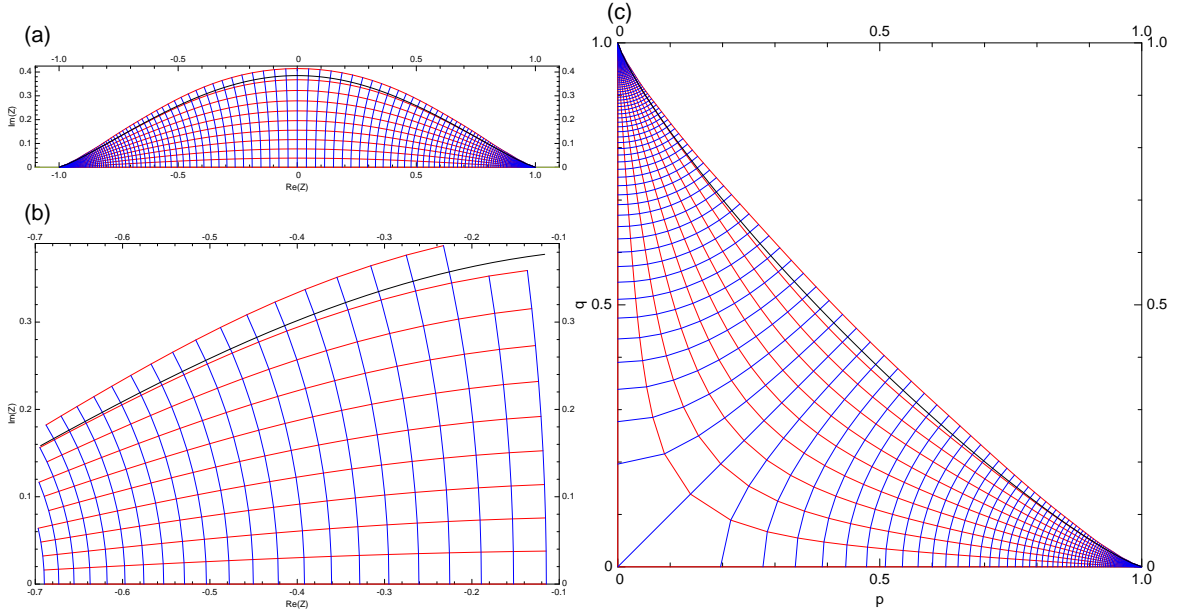


Figure 3. In this extreme example of a fat bicorn, constructed to make approximation by asymptotic mean very hard, we see that, in this case of the zeroth-order approximation, there is indeed a sizeable mismatch between the edge of the solution and the prescribed boundary of the bicorn. The Z -plane solution in its entirety is shown in panel(a), and an expanded view of a portion of it, to more clearly show the mismatch, is provided in (b). Panel (c) shows the corresponding bicorn region itself, corresponding to the views shown in the two panels of Fig. 2.

with corresponding generalizations of the recursion to higher orders if required. The numerical coefficients for these first two vectors are:

$$\mathbf{H}_{(2)} = \left[\frac{1}{6} \quad -\frac{1}{3} \right]^T \quad (4.26a)$$

$$\mathbf{H}_{(4)} = \left[\frac{7}{360} \quad -\frac{2}{45} \quad -\frac{1}{30} \quad -\frac{2}{15} \quad \frac{1}{5} \right]^T. \quad (4.26b)$$

Recalling the definitions of the derivative vectors \mathbf{D} , the fourth order formula written out explicitly becomes,

$$\begin{aligned} \frac{dX_0}{dx} \Big|_{x=0} \equiv a_1 = \hat{Y}_1 \left[1 + \frac{1}{6} \hat{Y}_1 \frac{d^2 \hat{Y}_1}{dX_1^2} - \frac{1}{3} \left(\frac{d\hat{Y}_1}{dX_1} \right)^2 + \frac{7}{360} \hat{Y}_1^3 \frac{d^4 \hat{Y}_1}{dX_1^4} - \frac{2}{45} \hat{Y}_1^2 \frac{d^3 \hat{Y}_1}{dX_1^3} \frac{d\hat{Y}_1}{dX_1} \right. \\ \left. - \frac{1}{30} \hat{Y}_1^2 \left(\frac{d^2 \hat{Y}_1}{dX_1^2} \right)^2 - \frac{2}{15} \hat{Y}_1 \frac{d^2 \hat{Y}_1}{dX_1^2} \left(\frac{d\hat{Y}_1}{dX_1} \right)^2 + \frac{1}{5} \left(\frac{d\hat{Y}_1}{dX_1} \right)^4 \right] + \mathcal{O}(\lambda^6). \quad (4.27) \end{aligned}$$

As suggested in the next section, it is unlikely that any further practical numerical benefit would result from extending the asymptotic expansion to higher orders except in very special cases; nevertheless, we list these, and the next two orders of the \mathbf{H} coefficients, together with their associated partitions, in Table 2 (although we don't attempt to give algebraic details for these higher order extensions).

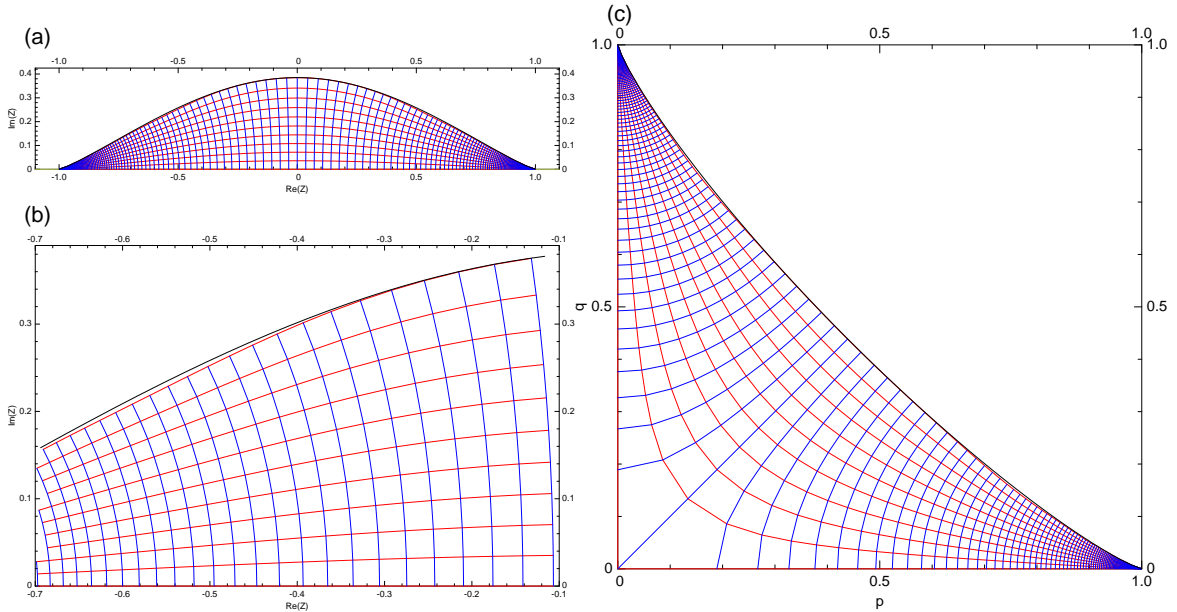


Figure 4. Like Fig. 3 except with the use of the first additional asymptotic approximation terms of (4.23).

5. Idealized examples

If we take the function,

$$q = 1 - [1 - (1 - p)^\alpha]^{1/\alpha} \quad (5.1)$$

for some exponent α greater than 1, then the region for q below the graph of this function in a cartesian (p, q) plot for $p \in [0, 1]$ defines an idealized and simple bicorn region. if we take for our exponent the intermediate value, $\alpha = 4$, the reconstructed conformal mapping result obtained for the asymptotic approximation correct to order λ^2 is already excellent. In Fig. 2 is shown the zeroth-order estimate using $dX_0(0)/dx = a_1 \approx \hat{Y}_1$ in panel (a), where a small mismatch can be seen between the solution edge and the defined boundary curve (black). The correction to order λ^2 is shown in right panel, (b).

In order to see any further effect of the higher-order correction, we need to consider a more extreme test of the method, which is provided by the choice of the exponent, $\alpha = 1.2$. Although the shape of this bicorn no longer resembles anything we would expect to see in a conformal oversight grid configuration, it more clearly displays the effects of the higher orders of expansion. In Fig. 3 we show the zeroth-order solution for the Z -plane region in panel (a) and, a magnified portion of the same solution, in panel (b). The bicorn solution is now shown in panel (c), and the boundary mismatch is very obvious.

When we apply the asymptotic correction (4.23) accurate to order λ^2 the improvement, shown in Fig. 4 in the same style, is evident, but a mismatch is still visible. Finally, with the fully order- λ^4 -accurate approximation that uses the additional terms of (4.24), we see in Fig. 5 that the resulting mismatch between the solution edge and the prescribed boundary curve is hardly visible at all. We need to be aware, though, that the expansion in even powers of λ that

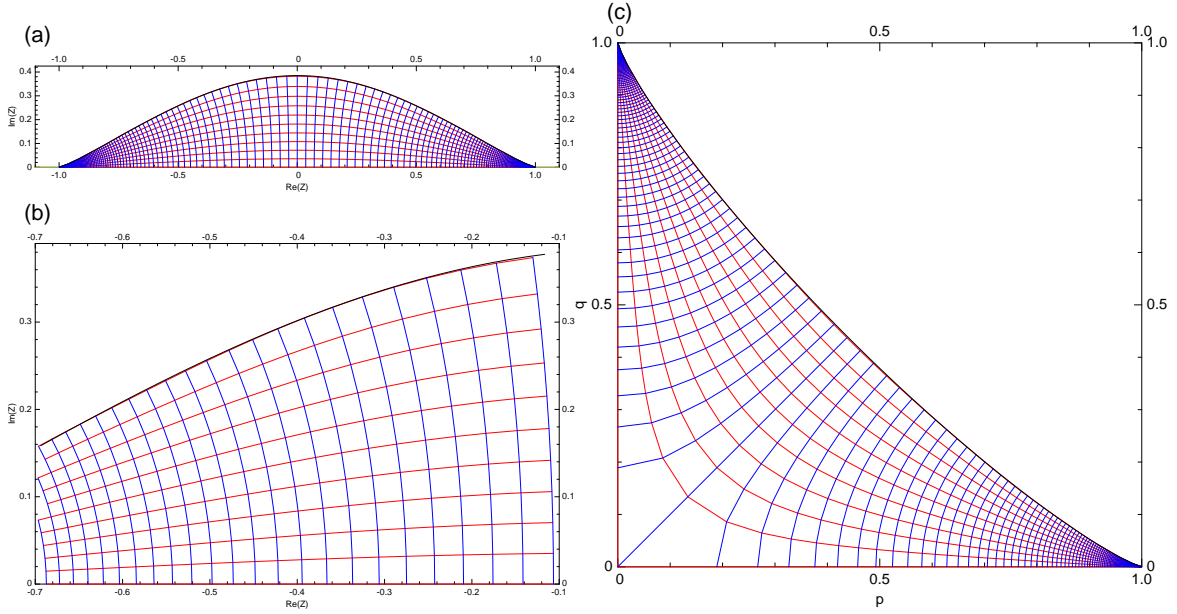


Figure 5. Like Figs. 3 and 4 but with the additional terms in the asymptotic series given by (4.24) (or equivalently, by (4.27)).

we are using is asymptotic, and not convergent; extending the series to higher powers might not necessarily always reduce the residual error, and the numerical evaluation of the higher order derivatives of the boundary curve to a sufficient accuracy necessitated by such higher order asymptotic expansions becomes extremely difficult in practice.

6. Discussion and Conclusion

It is important to emphasize that the construction of the blending weights, although seemingly involving a complicated sequence of computations, needs only to be done once – at the same time that the grid itself is constructed. The blending weights at the two overlapping grids in a representative bicorn region are then stored for use over the duration of the forecast run, and *using* these complementary weights is a relatively trivial matter of multiplying each of the pair of fields or fluxes, interpolating, summing, and possibly instituting some form of constraint-restoration to ensure conservations (this will be described more fully in Purser and Rančić , 2020).

The fact that the weighting function, described in the Introduction as an incomplete beta function of y , has very slack gradients at both sides ($y = 0$ and $y = 1$) of the bicorn region, means that the remaining positional discrepancy at of the solution edge at $y = 1$ translates into a very much tinier discrepancy in the weight W itself. Thus, although it is not too difficult to employ the Fourier machinery iteratively to refine our trivially-computed asymptotic approximate solution, it is almost certainly not worth the effort and extra computational time in practice.

TABLE 2. COEFFICIENTS H UP TO ORDER λ^8

π	H	π	H
2	$\frac{1}{6}$	8	$\frac{127}{604800}$
1, 1	$-\frac{1}{3}$	7, 1	$\frac{1}{315}$
4	$\frac{7}{360}$	6, 2	$\frac{53}{18900}$
3, 1	$-\frac{2}{45}$	5, 3	$-\frac{19}{4725}$
2, 2	$-\frac{1}{30}$	4, 4	$-\frac{11}{3024}$
2, 1, 1	$-\frac{2}{15}$	6, 1, 1	$\frac{317}{37800}$
1, 1, 1, 1	$\frac{1}{5}$	5, 2, 1	$-\frac{121}{6300}$
6	$\frac{31}{15120}$	4, 3, 1	$-\frac{167}{1890}$
5, 1	$\frac{11}{1260}$	4, 2, 2	$-\frac{149}{2520}$
4, 2	$-\frac{1}{168}$	3, 3, 2	$-\frac{107}{1260}$
3, 3	$-\frac{19}{1260}$	5, 1, 1, 1	$-\frac{8}{1575}$
4, 1, 1	$-\frac{9}{280}$	4, 2, 1, 1	$-\frac{97}{1260}$
3, 2, 1	$-\frac{19}{126}$	3, 3, 1, 1	$-\frac{2}{45}$
2, 2, 2	$-\frac{41}{840}$	3, 2, 2, 1	$-\frac{11}{315}$
3, 1, 1, 1	$\frac{26}{315}$	2, 2, 2, 2	$\frac{37}{2520}$
2, 2, 1, 1	$\frac{13}{70}$	4, 1, 1, 1, 1	$\frac{11}{252}$
2, 1, 1, 1, 1	$\frac{19}{210}$	3, 2, 1, 1, 1	$\frac{121}{315}$
1, 1, 1, 1, 1, 1	$-\frac{1}{7}$	2, 2, 2, 1, 1	$\frac{443}{1260}$
		3, 1, 1, 1, 1, 1	$-\frac{4}{35}$
		2, 2, 1, 1, 1, 1	$-\frac{3}{7}$
		2, 1, 1, 1, 1, 1, 1	$-\frac{16}{315}$
		1, 1, 1, 1, 1, 1, 1, 1	$\frac{1}{9}$

The problem we have addressed here, conformally mapping a given region to a parallel-sided strip, also occurs (though usually in slightly more general form, without the one straight edge) in the semigeostrophic theory of two-dimensional frontogenesis in an atmosphere of uniform potential vorticity, as shown in the work of Hoskins (1971) and Hoskins and Bretherton (1972). It seems very likely, therefore, that a minor generalization of the asymptotic technique described here could be made to apply also to the problem of finding approximate semigeostrophic solutions. We return to this analogy below.

The adaptation of the Phillips (1957) three-map overset configuration in which the pole-centered grids are (conformal) polar-stereographic, and the equatorial grid is the (conformal) Mercator, has two distinct annular overlap regions with four right-angular corners on only one side of each overlap band. When we view this overlap from the Cartesian coordinate frame of the polar grid, the edge of the overlap that remains smooth is simply the circle just inside the square boundary of the polar grid, as shown in panel (a) of Fig. 6. In this case, the way to transform away the right angles is to apply the Schwarz-Christoffel transformation from an upper complex half-plane, z , with pre-images of the corners taken to be the points on the real

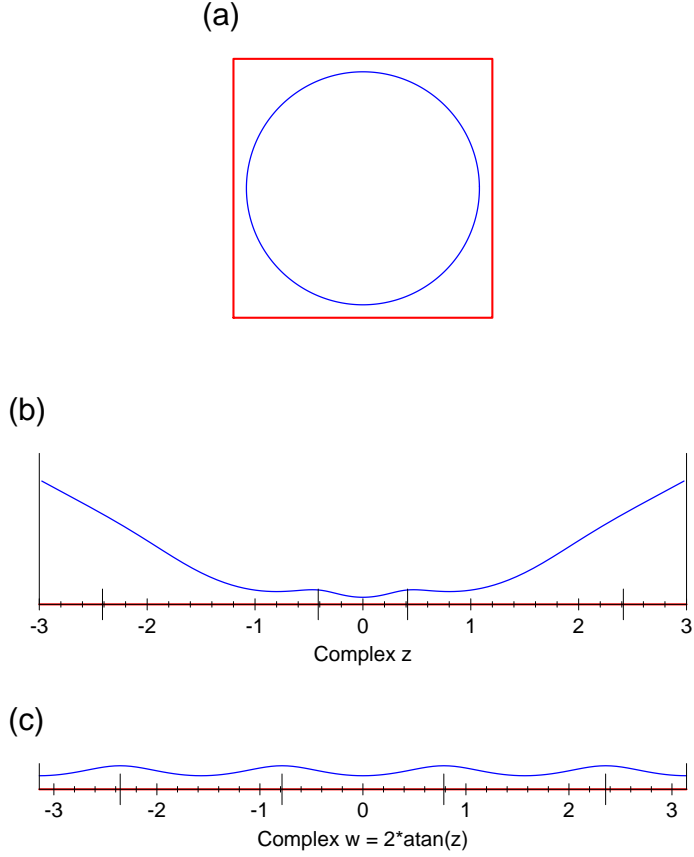


Figure 6. The case of the three-map Phillips (1957) style of fully overset grids involving a central cylindrical map sandwiched between polar-stereographic maps can have their two overlap regions equipped with a solution to the Laplace equation from which we derive a smooth blending function as before. From the square frame of one of the polar maps, the boundary of the equatorial map forms a circle just inside, as shown in panel (a). This configuration, when placed just above the real axis of a complex plane, can be regarded as the image of the elliptic integral (6.1) from the complex z -plane configuration shown in panel (b), where the singular pre-images of the four corners of the polar grid are indicated by the tall vertical dashes cutting the real axis. In order to further transform the overlap region into one which is suitable for Fourier analysis, we take the complex atan transformation to the complex w -plane where the corresponding configuration is shown in panel (c), and the expected four-wave periodicity is readily seen.

axis, $Z_1 = -1/p$, $Z_2 = -p$, $Z_3 = +p$ and $Z_4 = +1/p$, with $p = \sqrt{2} - 1$. This transformation:

$$q = C \int_0^Z \prod_{i=1}^4 \frac{1}{(t - Z_i)^{1/2}} dt = C \int_0^Z \frac{1}{[(t^2 - p^2)(t^2 - 1/p^2)]^{1/2}} dt, \quad (6.1)$$

is essentially an ‘elliptic integral of the first kind’ (Whittaker and Watson, 1902). We find that the pre-image of the circular inner boundary of the overlap maps to a large smooth loop in the z plane, a portion of which is shown (in blue) in panel (b) of the figure. In order to make the overlap conveniently cyclic for Fourier analysis, we can apply the further analytic (and therefore conformal) transformation,

$$w = 2\arctan(z), \quad (6.2)$$

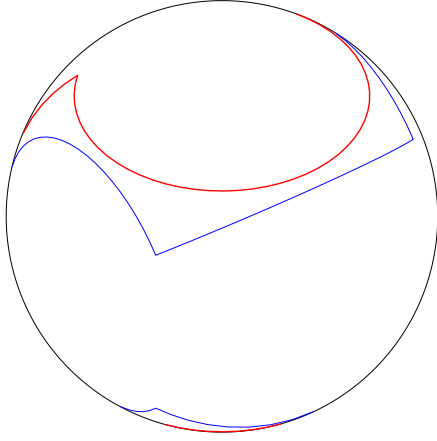


Figure 7. A sketch of the configuration on the sphere of the boundary rectangles of the mutually overlapping ‘Yin-Yang’ grids.

where the complex form of this function is employed. This results in the w -plane mapping of the overlap shown in panel (c), and it is periodic in $\text{Real}(w)$ with four identical waves spanning the periodic interval $[-\pi, \pi]$ of this mapping. Clearly, the solution of the Laplace equation by the methods discussed in the previous sections of this note should present us with no difficulty in this case.

A much more challenging problem arises when we consider how the Laplace equation might be solved in the case of the Yin-Yang grid of Kageyama and Sato (2004), where two congruent rectangular regions overlap in transverse orientations so that the boundary of one lies just inside the rectangle of the other, mutually, as shown in the sketch of Fig. 7, where each is given a margin sufficient to maintain a nonvanishing width of overlap all around. The image of the boundary of one map (blue) is shown in the Cartesian frame of the other (red) in panel (a) of Fig. 8. In this case the elliptic integral (6.1) is still valid, but the value of p that determines the preimages of the corners needs to be found (by a separate suitable iteration, typically) to ensure that the image is a rectangle of the correct aspect ratio. For a long rectangle, this places the pre-images in closely clustered pairs, as we see in the panel (b) of this figure, and the result now is that the pre-image of the inner boundary (blue) of the overlap possesses deep ‘notches’ where the thickness of the z -plane overlap domain is reduced by orders of magnitude. The corners of the overlap region are only removed on one edge of the overlap. Again, the application of the further mapping using (6.2) to the complex w -plane makes the overlap region periodic, (panel (c)) and therefore amenable to treatment by ordinary Fourier methods, but the angular boundary curve makes the solution procedure much harder than in previous examples.

One approach to solving the Laplace equation in this example would be to estimate the position of the median $y = 1/2$ contour of the potential spanning $y = 0$ on the ‘outer’ (red) boundary, and $y = 1$ on the ‘inner’ angular (blue) boundary of the annular overlap. Then solve the Laplace problem with this interim solution, and use the symmetry between the two congruent domains to transform the symmetric image of this solution, originally for the $y < 1/2$ portion, into the corresponding image of the $y > 1/2$ portion, and record the integrated mismatch of both components of the complex-valued solution of both versions of this median

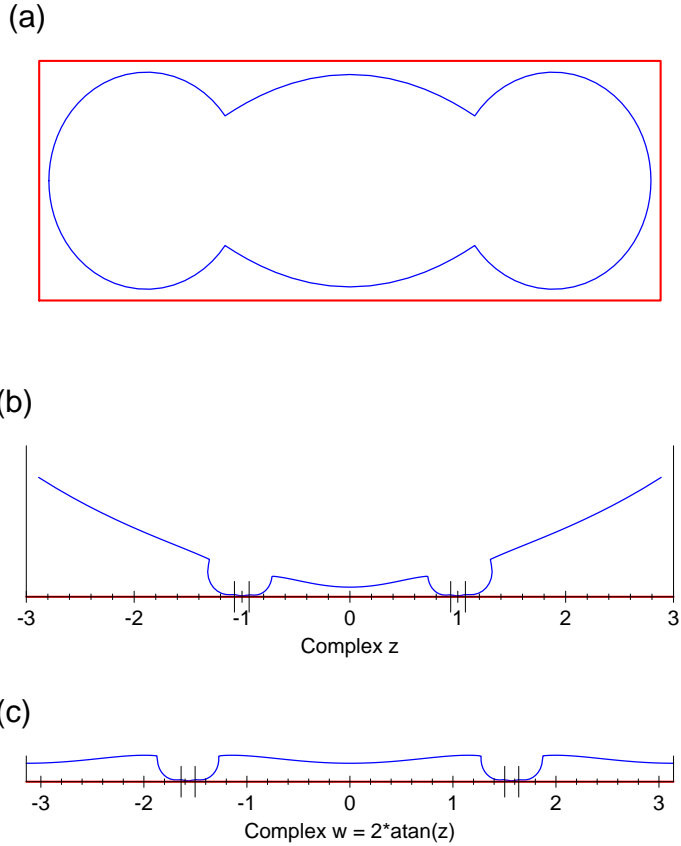


Figure 8. The case of the overlap region of the Yin-Yang grid, whose shape in the frame of one of the conformal maps is the annular band bounded by the red rectangle on the outside and the image of the congruent rectangle whose boundary (blue) is contained inside it, is shown in panel (a). The pre-image of the elliptic integral with the correct choice of the parameter, p , for this aspect ratio leads to the picture shown in panel (b). This is made periodic by the further transformation to the w -plane by the application of the complex function (6.2) as before, but the difficulty of the angular boundary (the blue curve) remains to be dealt with by a more involved procedure.

curve, as an integrated squared-distance cost function. Then we can minimize this mismatch with respect to variations in the Fourier expansion coefficients that define our Laplace equation solution, as well as with respect to the ‘modulus’, or period, of the solution. In this way, we can avoid direct numerical involvement with the right-angles that remain on the $y = 1$ side of the solution, and a consistent solution can be found when the mismatch becomes negligible. Returning to the semigeostrophic analogy again, it would seem that this more general problem of finding the conformal mapping to a constant-width annular strip bears some similarities, computationally at least, to the problem of finding solutions in two-dimensional semigeostrophic theory that involve *two* stratified layers of different constant potential vorticities, one lying above the other, which Hoskins and collaborators also studied in the context of a ‘stratosphere’ overlying a ‘troposphere’; in which case, it is necessary to match the locations of points along the common interface, computed separately from the equations governing the solutions of the two different air masses, which is analogous to the median-matching problem we have with the

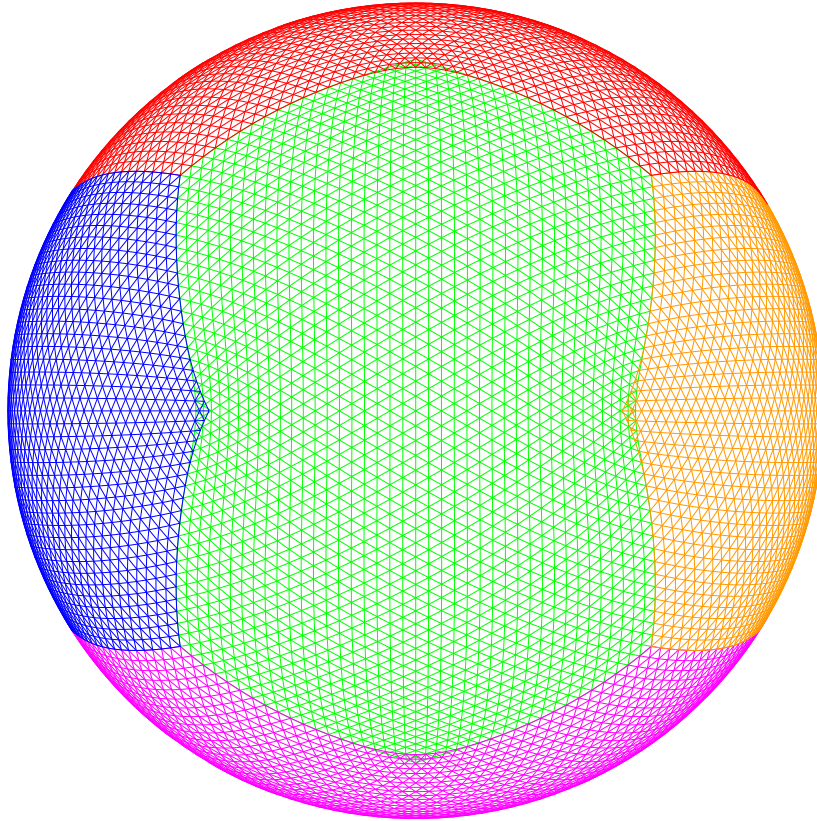


Figure 9. An example of a conformal overset grid based on icosahedral geometry. The symmetry is broken by the overlapping regions to what is known as “pyritohedral symmetry”.

Yin-Yang overlap.

Finally, we note that the Riemann surface conformal overset grid, or the traditional patterns of overset grids, also have forms adapted to *triangular* meshes. As an example, Fig. 9 shows how to modify a conformal icosahedral grid (with 12 vertex regions) to a corresponding Riemann-surface conformal overset grid where the high symmetry (order 120) of the original icosahedron is broken, by the necessity for oversets, to the lower ‘pyritohedral’ symmetry (of order 24). Again, the conformal overset version of the icosahedral grid eliminates the *strong* singularities that the unmodified conformal icosahedral grid possesses. One small difference from the cubic case is that the icosahedral bicorn regions have corners making an internal angle of 120° instead of 90° , so the necessary exponent in the complex power transformation needed to remove them is $3/2$ instead of 2.

Acknowledgments

This work described in this note has benefitted from the encouraging support of, and discussions with, Dr. Misha Rančić. The author is also grateful for the internal reviews of Drs. Sajal Kar and Henry Juang, which helped to improve the presentation.

References

- Abramowitz, M., and I. A. Stegun 1972 *Handbook of Mathematical Functions with Formulas, Graphs, and Mathematical Tables.*, Dover, New York. 1046 pp.
- Beardon, A. F. 1983 *The Geometry of Discrete Groups* Springer, New York.
- Browning, G. L., J. J. Hack, and P. N. Swarztrauber 1989 A comparison of three numerical methods for solving differential equations on the sphere. *Mon. Wea. Rev.*, **117**, 1058–1075.
- Chesshire, G., and W. Henshaw 1990 Composite overlapping meshes for the solution of partial differential equations. *J. Comput. Phys.*, **90**, 1–64. doi:10.1016/0021-9991(90)90196-8.
- Driscoll, T. A., and L. N. Trefethen 2002 *Schwarz-Christoffel Mapping*, Cambridge University Press, Cambridge, UK. 132 pp.
- Hoskins, B. J. 1971 Atmospheric frontogenesis models: Some solutions. *Quart. J. Roy. Meteor. Soc.*, **97**, 139–153.
- Hoskins, B. J., and F. P. Bretherton 1972 Atmospheric frontogenesis models: mathematical foundation and solution. *J. Atmos. Sci.*, **29**, 11–37.
- Janjić, Z. I., and R. Gall 2012 Scientific documentation of the NCEP nonhydrostatic multiscale model on the B grid (NMMB) Part I: Dynamics. NCAR Tech. Note. NCAR/TN-489+STR. 75 pp., doi:10.5065/D6WH2MZX.
- Kageyama, A., and T. Sato 2004 The “Yin-Yang grid”: An overset grid in spherical coordinates. *Geochem., Geophys. Geosyst.*, **5**, Q09005, doi:10.1029/2004GC000734.arXiv.org:physics/0403123
- Krantz, S. G., 2016 *The theory and practice of conformal geometry*. Doever, New York.
- McGregor, J. L. 1996 Semi-Lagrangian advection on conformal-cubic grids. *Mon. Wea. Rev.*, **124**, 1311–1322.
- Napier, T., and M. Ramachandran 2011 *An Introduction to Riemann Surfaces* Springer, New York.
- Phillips, N. A. 1957 A map projection system suitable for large-scale numerical weather prediction. *J. Meteor. Soc. Japan, 75th Anniversary Volume*. 262–267.
- Purser, R. J., and Rančić, M. 1998 Smooth quasi-homogeneous gridding of the sphere. *Quart. J. Roy. Meteor. Soc.*, **124**, 637–647.
- Purser, R. J., and Rančić, M. 2020 Technique for the construction of quasi-uniform conformal overset grids on the sphere based on polyhedral frameworks. NOAA/NCEP Office Note (In preparation).
- Putman, W. M., and S.-J. Lin 2007 Finite-volume transport on various cubed-sphere grids. *J. Comput. Phys.*, **227**, 55–78.
- Rančić, M., R. J. Purser, and F. Mesinger 1996 A global shallow-water model using an expanded spherical cube: Gnomonic versus conformal coordinates. *Quart. J. Roy. Meteor. Soc.*, **122**, 959–982.
- Rančić, M., R. J. Purser, D. Jovic, R. Vasic, and T. Black 2017 A nonhydrostatic multiscale model on the uniform Jacobian cubed sphere. *Mon. Wea. Rev.*, **145**, 1083–1105.
- Sadourny, R. 1972 Conservative finite-differencing approximations of the primitive equations on quasi-uniform spherical grids. *Mon. Wea. Rev.*, **100**, 136–144.
- Starius, G. 1980 On composite mesh differencing methods for hyperbolic differential equations. *Numer. Math.*, **35**, 241–255.

- Weyl, H. 2009 *The Concept of a Riemann Surface, 3rd Ed.* Dover, New York.
- Whittaker, E. T., and G. N. Watson 1902 *A Course of Modern Analysis.* Cambridge University Press,